



Atmospheric Correction for Polarimetric Images Based on Spectral Segregation

Pu Xia

Key Laboratory of Spectral Imaging Technology, Xi'an Institute of Optics and Precision Mechanics, Chinese Academy of Sciences, Xi'an 710119, China
xiapu@opt.ac.cn

Xiaolai Chen*

Key Laboratory of Spectral Imaging Technology, Xi'an Institute of Optics and Precision Mechanics, Chinese Academy of Sciences, Xi'an 710119, China
laililai@opt.ac.cn

Zhaohuan Tang

China National Heavy Machinery Research Institute Co., Ltd., Xi'an 710018, China
tangzhaohuan@sino-heavytech.com

ABSTRACT

In hazy weather, light's penetration power is wavelength related, the longer wavelength, the less attenuation. Although traditional polarimetric image-dehazing algorithms have demonstrated their ability in enhancing grayscale images, but their ignorance of the spectral difference will lead to serious color distortion when utilizing these algorithms for color images. To conquer that problem, we propose a new method base on spectral segregation. 15 spectral bands are selected and dehazed with the polarimetric dehazing algorithm separately to obtain the best dehazing effects. The blue, green and red channels of the dehazed image, which are acquired through image fusion of the spectral bands, are adjusted with different coefficients to correct the color distortion. 10 infrared bands are added to the short-wavelength channels to enhance the details of the objects especially the trees. Experiment and data analysis demonstrate the effectiveness of our method in increasing visibility and preserving color information. The amount of color distortion can be reduced by 89.6% compared with the polarimetric image-dehazing algorithm without spectral segregation.

CCS CONCEPTS

• Computing methodologies; • Computer graphics; • Theory of computation; • Design and analysis of algorithms; • Applied computing; • Computers in other domains;

KEYWORDS

Image processing, Haze removal, Color image restoration, Polarimetric imaging, Spectral analysis

ACM Reference Format:

Pu Xia, Xiaolai Chen*, and Zhaohuan Tang. 2022. Atmospheric Correction for Polarimetric Images Based on Spectral Segregation. In *2022 the 6th International Conference on Innovation in Artificial Intelligence (ICIAI) (ICIAI 2022), March 04–06, 2022, Guangzhou, China*. ACM, New York, NY, USA, 5 pages. <https://doi.org/10.1145/3529466.3529479>

Permission to make digital or hard copies of all or part of this work for personal or classroom use is granted without fee provided that copies are not made or distributed for profit or commercial advantage and that copies bear this notice and the full citation on the first page. Copyrights for components of this work owned by others than ACM must be honored. Abstracting with credit is permitted. To copy otherwise, or republish, to post on servers or to redistribute to lists, requires prior specific permission and/or a fee. Request permissions from permissions@acm.org.

ICIAI 2022, March 04–06, 2022, Guangzhou, China

© 2022 Association for Computing Machinery.

ACM ISBN 978-1-4503-9550-2/22/03...\$15.00

<https://doi.org/10.1145/3529466.3529479>

1 INTRODUCTION

For the past few years, the average AQI (air quality index) of densely populated areas in China has continued to rise especially in first-tier cities like Beijing and Shanghai [1] due to the worsening air pollution [2]. The atmospheric scattering caused by haze will lead to the declination of contrast and visibility of the image captured in hazy weather which will make it inconvenient for observation or image processing [3]. These potentialities have motivated the development of polarimetric image-dehazing methods [4–6].

The polarimetric image-dehazing methods [3], unlike the prior information based methods which need prior information about the imaged scene like distances [7] or images took on different weather conditions [8], can fulfill the requirements of real-time dehazing. The polarization-based methods also have superior dehazing effect over pure image enhancement methods [9, 10] which will induce an inevitable loss of detailed information due to the lack of physical model of atmospheric scattering. Traditional polarization-based methods, although have been proven to be effective in image dehazing, ignore the spectral difference of penetration power of the incident light which will lead to serious color distortion. Based on our previous study [11, 12], the ability of light to penetrate the hazy particles is related with wavelength, the longer wavelength the less attenuation. Therefore, images in near-infrared bands have better clarity in hazy weather. Traditional image-dehazing method process the three color channels: the blue, the green and the red with the same algorithm leaving the dehazing result of the blue channel worse than the other two. According to the dark channel theory [13], the brightness of the blue channel will be higher leaving the dehazed image blue-shifted [5, 6].

To solve the problem of color distortion, we present a method that separately processes the different spectral channels of the imaged scene. Due to the relation of light's penetration power with wavelength, our method increases the dehazing strength of the short-wavelength bands and decreases the dehazing strength of the long-wavelength bands to balance the dehazing level. Infrared bands are added to the blue and the green channels to further correct the blue-shift. The dehazing result is obtained through image fusion of the spectral bands. The addition of infrared bands will also enhance the details of the dehazed image.

2 PRINCIPLES AND METHOD

Based on the aforementioned facts, the spectral difference enables the decomposition of the dehazing process. 15 visible bands are chosen to be dehazed, 5 bands for each channel. In conjunction with

the decomposition, a polarimetric dehazing algorithm is needed for each band. Based on our atmospheric scattering model [3, 11, 12], the total intensity of the image radiance I received by the sensor in hazy weather can be divided into two parts:

$$I = D + A, \quad (1)$$

where D is the direct transmission of radiance from the imaged scene which is non-polarized and A is the airlight scattered by atmosphere which is partial polarized. The airlight A is the unwanted interference. The direct transmission D is the object radiance L after attenuation which is the information we need. The proposed method utilizing the polarimetric difference of D and A to separate the interference A and compensate for the attenuation of D . D decreases with observation distance which can be expressed as

$$D = L \cdot e^{-\beta z}, \quad (2)$$

where $e^{-\beta z}$ is the transmittance of atmosphere [14], z is the observation distance, β is the scattering coefficient which is assumed to be distance invariant. The airlight A increases with observation distance according to

$$A = A_\infty \left[1 - e^{-\beta z} \right] \quad (3)$$

where A_∞ is the airlight radiance corresponding to an object at an infinite distance.

The dehazing algorithm proposed by Schechner et al. [15] calculates L by

$$L = \frac{I - A}{1 - A/A_\infty},$$

$$= \frac{I^\perp + I^\parallel - (I^\perp - I^\parallel) / p}{1 - (I^\perp - I^\parallel) / p A_\infty} / p \quad (4)$$

where I^\perp is the image representing the beat state of the polarizer, I^\parallel is the image representing the worst state of the polarizer, p is the degree of polarization of A . Manual operation and subjective evaluation is needed during data collection which is unable to meet the requirements of real-time dehazing.

Our algorithm employs the Stokes vector to solve the above problem, the first element S_0 represents the total radiance received by the sensor, the second and third elements S_1 and S_2 represent the linear polarimetric characteristic of the incident light. Then the angle of polarization representing the best and worst state of the polarizer θ^\perp and θ^\parallel could be calculated by

$$\theta^\perp = \frac{1}{2} \arctan \frac{S_2}{S_1}, \quad (5)$$

$$\theta^\parallel = \theta^\perp + \frac{\pi}{2}, \quad (6)$$

Then we calculate I^\perp and I^\parallel employing the Mueller matrix which can be expressed as

$$I^\perp = \frac{1}{2} (S_0 + S_1 \cos 2\theta^\perp + S_2 \cos 2\theta^\perp), \quad (7)$$

$$I^\parallel = \frac{1}{2} (S_0 + S_1 \cos 2\theta^\parallel + S_2 \cos 2\theta^\parallel), \quad (8)$$

We need to estimate p and A_∞ to complete the dehazing algorithm. Under the assumption that $e^{-\beta z}$ in the sky is zero, p and A_∞ can be estimated using the region in the image that represents the sky. An automatic algorithm on the basis of the polarization

measurements of the original images is used to extract the sky region, the estimated p and A_∞ can be given by

$$p = \frac{1}{\Omega} \sum_{(x,y) \in \Omega} \left[\frac{I^\parallel(x,y) - I^\perp(x,y)}{I^\perp(x,y) + I^\parallel(x,y)} \right], \quad (9)$$

$$A_\infty = \frac{1}{\Omega} \sum_{(x,y) \in \Omega} \left[I^\perp(x,y) + I^\parallel(x,y) \right], \quad (10)$$

where Ω represents the number of pixels in the sky region, (x, y) is the coordinates of the sky pixels. Under more normal circumstances, scattering particles of large radius like the water droplets will absorb the energy from the incident light and become light sources which will generate secondary radiance [16]. Two correction factors are introduced to revise p and A_∞ to perfect our atmospheric scattering model, which are given by

$$p_c = p \cdot \varepsilon_1, \quad (11)$$

$$A_{\infty c} = A_\infty \cdot \varepsilon_2, \quad (12)$$

where p_c and $A_{\infty c}$ are the corrected p and A_∞ . The value of ε_1 should be $1 < \varepsilon_1 < 1/p$, meanwhile, the value of ε_2 should make sure that $A_{\infty c} < S_0$.

In a color image, the blue channel is 440nm-485nm, the green channel is 500nm-565nm, the red channel is 625nm-740nm. Five visible bands are selected for each channel with spectral interval of 6nm, 460.3nm, 530.3nm and 680.7nm are the center bands for the blue, green and red channels respectively. Coefficients are added to each spectral band to balance the dehazing level of the three color channels: B , G and R which can be given by

$$B = (L_{449.9nm} + L_{455.9nm} + L_{461.8nm} + L_{467.8nm} + L_{473.7nm}) \times C_B,$$

$$C_B = (0.1, 0.15, 0.2, 0.25, 0.3)^T \quad (13)$$

$$G = (L_{519.9nm} + L_{525.8nm} + L_{531.8nm} + L_{537.8nm} + L_{543.7nm}) \times C_G,$$

$$C_G = (0.1, 0.2, 0.3, 0.2, 0.1)^T \quad (14)$$

$$R = (L_{668.8nm} + L_{674.8nm} + L_{680.7nm} + L_{686.7nm} + L_{692.6nm}) \times C_R,$$

$$C_R = (0.3, 0.25, 0.2, 0.15, 0.1)^T \quad (15)$$

where $L_{449.9nm} - L_{692.6nm}$ are the dehazing results of 449.9nm-692.6nm, C_B , C_G and C_R are the image fusion coefficients for the blue, green and red channels.

Infrared bands are added to the blue and the green channels to further correct the color distortion and enhance details. Due to the seriousness of noise, 10 infrared bands: 895.2nm, 896.6nm, 898.1nm, 899.6nm, 901.1nm, 902.6nm, 904.1nm, 905.6nm, 907.1nm and 908.6nm are superimposed to increase the SNR which can be given by

$$NIR = 0.1 \times \sum I_{NIR}, \quad (16)$$

where NIR is the superimposing result of the infrared bands, I_{NIR} represents the 10 infrared bands after dehazing. The enhanced blue channel B_{en} and green channel G_{en} can be given by

$$B_{en} = B + 0.3 \times NIR, \quad (17)$$

$$G_{en} = G + 0.15 \times NIR, \quad (18)$$

The blue, green and red channels will be fused to lead to a well-restored color dehazing result.

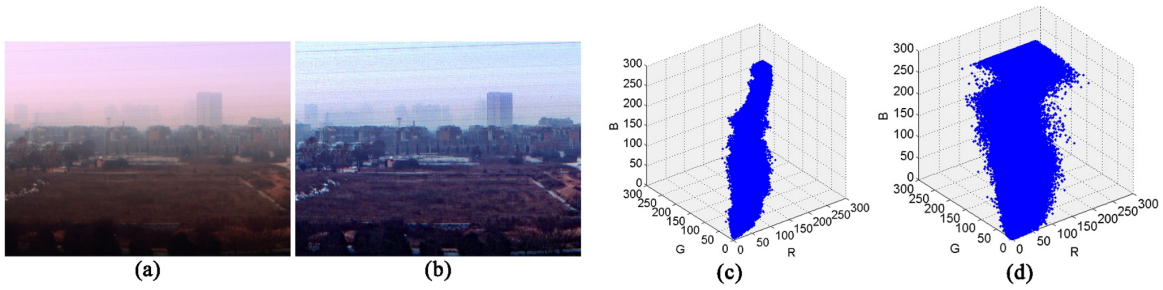


Figure 1: (a) The original image. (b) The dehazed image only by polarimetric dehazing algorithm. (c) The RGB distribution of the original image. (d) The RGB distribution of the dehazed image.

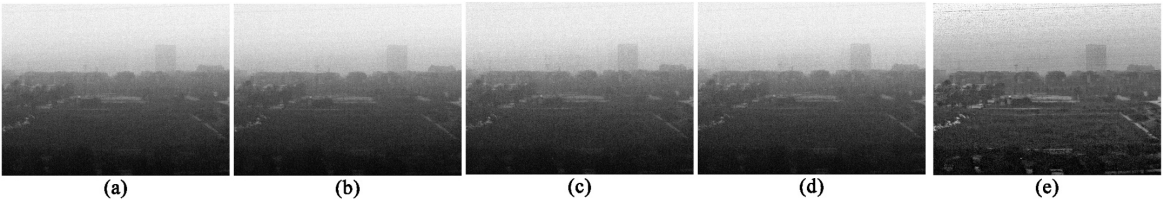


Figure 2: (a)/(b)/(c)/(d) The raw images of $0^\circ/45^\circ/90^\circ/135^\circ$ polarizer orientation angle of 461.8nm. (e) The dehazed image of 461.8nm.

3 EXPERIMENT RESULTS

The raw data was captured on building 2 of Xi'an Institute of Optics and Precision Mechanics in Xi'an, Shaanxi Province, China using a polarimetric spectral imager with 380nm-1000nm's spectral bandwidth and 1.5nm spectral resolution. This experiment was conducted in hazy weather with AQI of 193 [17] which indicates severe air pollution and poor visibility [1]. The spectrometer used in our experiments can work under normal color camera mode. The original image captured by our imager working under color model is shown in Figure 1(a), the dehazing result by the polarimetric dehazing algorithm without spectral segregation is shown in Figure 1(b). In Figure 1(b), more details could be observed after dehazing, but the whole image displays blue-shifted colors. RGB distribution is employed to get more quantitative data, the RGB distribution of Figure 1(a) and 1(b) are shown in Figure 1(c) and 1(d). The distribution area is enlarged but shifted to the blue axis which is in coordination with the above conclusion.

The original images and dehazing results of the center band for each color channel and the infrared band 901.1nm are demonstrated. The original polarized images of 461.8nm are shown in Figure 2(a)-2(d), Figure 2(e) shows the dehazed image with $\varepsilon_1 = 2.1$ and $\varepsilon_2 = 1.1$. The original polarized images of 531.8nm are shown in Figure 3(a)-3(d), Figure 3(e) shows the dehazed image with $\varepsilon_1 = 1.9$ and $\varepsilon_2 = 1.5$. The original polarized images of 680.7nm are shown in Figure 4(a)-4(d), Figure 4(e) shows the dehazed image with $\varepsilon_1 = 2.1$ and $\varepsilon_2 = 1.8$. The original polarized images of 901.1nm are shown in Figure 5(a)-5(d), Figure 5(e) shows the dehazed image with $\varepsilon_1 = 1.5$ and $\varepsilon_2 = 2.4$. Generally, the dehazed images clearly exhibit significant improvements in contrast over the original images on 461.8nm-901.1nm, the quality of the images before and after dehazing are

both increasing with wavelength which is in consonance with our results in [11, 12].

The proposed method acquires the color dehazed image through weighted fusion of the 25 bands. Figure 6(a) is the original color image captured by the imager, Figure 6(b) is the dehazed image by our method. The dehazed image demonstrates the effectiveness of our method through the enhancement on image contrast and good preservation of detailed information, the color information and the edges of the objects are well restored. Two regions in the scene are selected and magnified in Figure 6. The distance of the building in red rectangle A and the trees in yellow rectangle B are 860m and 321m respectively. Distance map is shown in Figure 7. The building in the dehazed image is much easier to recognize and many details not seen in the raw image emerge after the dehazing. Great improvements of details are achieved in the trees in area B.

The RGB distribution of the dehazed image by our method is shown in Figure 8. The distribution is wider compared with Figure 1(d) and has not shifted to the blue axis which means the proposed method has better ability in scattering correction and color preservation.

The amount of blue-shift AMT_{bs} is introduced to quantitatively evaluate the color distortion which is expressed as

$$AMT_{bs} = \frac{|DN_{blus} - DN_{avg}|}{DN_{avg}} \quad (19)$$

where DN_{blus} is the average DN value of the blue channel, DN_{avg} is the average DN value of the whole image. The AMT_{bs} of the original image shown in Figure 1(a) is 1.85%, the AMT_{bs} of the dehazed image shown in Figure 1(b) and 6(b) are 18.19% and 1.89% respectively. The color of the dehazed image by our method is well

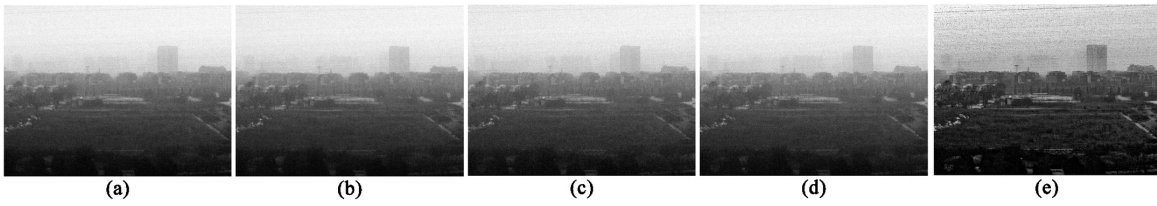


Figure 3: (a)/(b)/(c)/(d) The raw images of $0^\circ/45^\circ/90^\circ/135^\circ$ polarizer orientation angle of 531.8nm. (e) The dehazed image of 531.8nm.

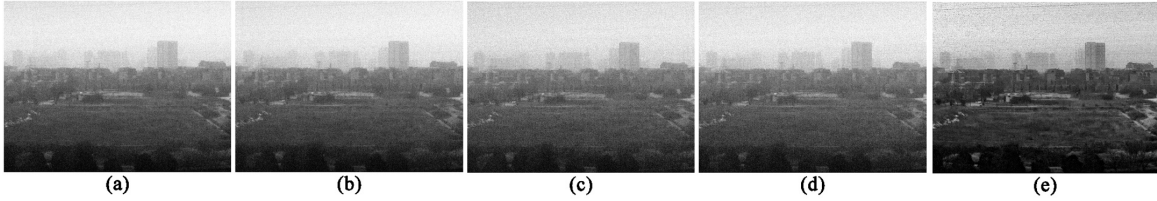


Figure 4: (a)/(b)/(c)/(d) The raw images of $0^\circ/45^\circ/90^\circ/135^\circ$ polarizer orientation angle of 680.7nm. (e) The dehazed image of 680.7nm.

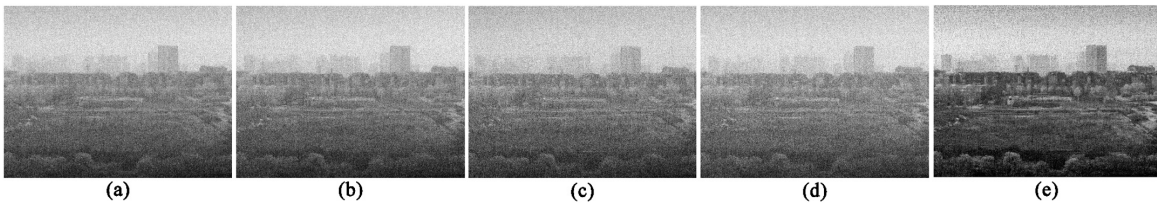


Figure 5: (a)/(b)/(c)/(d) The raw images of $0^\circ/45^\circ/90^\circ/135^\circ$ polarizer orientation angle of 901.1nm. (e) The dehazed image of 901.1nm.

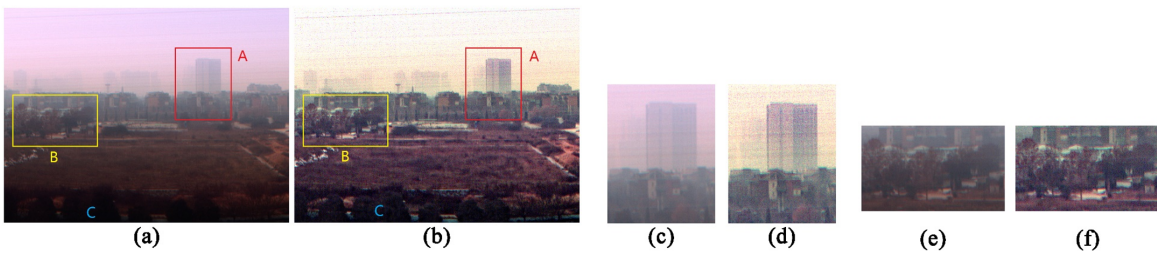


Figure 6: (a) The original color image. (b) The dehazed image by our method. (c) and (d) The red rectangle area before and after dehazing. (e) and (f) The yellow rectangle area before and after dehazing.

preserved and the amount of blue-shift can reduce by 89.6% compared with the polarimetric dehazing algorithm without spectral segregation.

4 CONCLUSIONS

In this paper, we analyze the strengths and weaknesses of the traditional polarimetric dehazing algorithms and explain the cause for blue-shift through spectroscopy. A new dehazing method utilizing both polarimetric and spectral information of the imaged scene is proposed. The dehazing process is separated into 25 different

spectral bands: 15 visible bands and 10 infrared bands. In order to balance the dehazing level, the dehazing strength of the short-wavelength bands are increased and that of the long-wavelength bands are decreased. The infrared bands are superimposed to reduce noise before being added to the blue and the green channels. The final dehazed image, which is obtained through weighted fusion, is well dehazed and has rich details. Comparison with the traditional polarimetric dehazing algorithm demonstrates its excellent ability in color retention. A parameter is proposed to quantitatively



Figure 7: Distance of the 2 marked areas in figure 6.

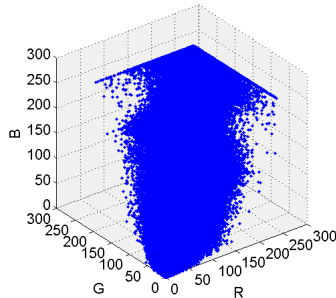


Figure 8: The RGB distribution of Figure 6(b).

evaluate the color distortion, experiment results indicate that our method can reduce the amount of blue-shift by 89.6%.

ACKNOWLEDGMENTS

This work was supported by the International Cooperation Program of China (2015DFA10140), National Nature Science Foundation of China (61905275), Western Lights Foundation of Chinese Academy of Sciences (XAB2017B23), and the Open Research Fund of CAS Key Laboratory of Spectral Imaging Technology.

REFERENCES

- [1] Jiajia Gao, Hezhong Tian, Ke Cheng, Long Lu, Mei Zheng, Shuxiao Wang, Jiming Hao, Kun Wang, Shenbing Hua, Chuanyong Zhu and Yong Wang. 2015. The variation of chemical characteristics of PM_{2.5} and PM₁₀ and formation causes during two haze pollution events in urban Beijing, China. *Atmospheric Environment* 107, 8(2015), 1-8.
- [2] Qianshan He, Guangqiang Zhou, Fuhai Geng, Wei Gao and Wei Yu. 2016. Spatial distribution of aerosol hygroscopicity and its effect on PM_{2.5} retrieval in East China. *Atmospheric Research* 170, 4(2016), 161–167.
- [3] Pu Xia, Xuebin Liu, and Peng Yan. 2016. Design and experiment of polarization dehazing imaging system. *Journal of Xidian University* 43, 2(2016), 104–109.
- [4] Tianquan Liang, Xiaobing Sun, Han Wang, Rufang Ti and Cumming Shu. 2016. Airborne Polarimetric Remote Sensing for Atmospheric Correction. *Journal of Sensors* 2016, 9(2016), 1-7.
- [5] Jian Liang, Liyong Ren, Enshi Qu, Bingliang Hu, and Yingli Wang. 2014. Method for enhancing visibility of hazy images based on polarimetric imaging. *Photonics Research* 2, 1(2014), 38-44.
- [6] Jian Liang, Liyong Ren, Haijuan Ju, Enshi Qu, and Yingli Wang. Visibility enhancement of hazy images based on a universal polarimetric imaging method. *Journal of Applied Physics* 116, 17(2014), 820-827.
- [7] John Oakley and Brenda Satherley. 1998. Improving image quality in poor visibility conditions using a physical model for contrast degradation. *IEEE Transactions on Image Processing* 7, 2(1998), 167–179.
- [8] Srinivasa Narasimhan and Shree Nayar. 2000. Chromatic framework for vision in bad weather. In *CVPR. IEEE*, 598–605.
- [9] Zhengguo Li and Jinghong Zheng. 2015. Edge-preserving decomposition-based single image haze removal. *IEEE Transactions on Image Processing* 24, 12(2015), 5432-5441.
- [10] Ko Nishino, Louis Kratz, and Stephen Lombardi. 2012. Bayesian defogging. *International Journal of Computer Vision* 98, 3(2012), 263–278.
- [11] Pu Xia and Xuebin Liu. 2016. Image dehazing technique based on polarimetric spectral analysis. *Optik* 127, 18(2016), 7350–7358.
- [12] Pu Xia and Xuebin Liu. 2017. Study on the polarization spectral image dehazing. *Spectroscopy and Spectral Analysis* 37, 8(2017), 2331-2338.
- [13] Kaiming He, Jian Sun, and Xiaoou Tang. 2011. Single image haze removal using dark channel prior. *IEEE Transactions on Pattern Analysis and Machine Intelligence* 33, 12(2011), 2341-2353.
- [14] Craig Bohren and Alistair Fraser. 1986. At what altitude does the horizon cease to be visible. *American Journal of Physics* 54, 3(1986), 222–227.
- [15] Yoav Schechner, Srinivasa Narasimhan, and Shree Nayar. 2003. Polarization-based vision through haze. *Applied Optics* 42, 3(2003), 511–525.
- [16] Yoav Schechner, Srinivasa Narasimhan, and Shree Nayar. 2001. Instant dehazing of images using polarization. In *CVPR. IEEE*, 325–332.
- [17] The AQI criterion can be read at <http://www.aqistudy.cn/>